Supporting Information

W. Wolff, [b] M. Dogan,[a] J. Basilio, [b] R. R. Oliveira,[c] T. Pfeifer,[a] and A. Dorn[a†]

[a] *Max Planck Institute for Nuclear Physics, Heidelberg, Germany.*
[*] *e-mail: alexander.dorn@mpi-hd.mpg.de*
[b] *Physics Institute, Federal University of Rio de Janeiro, Rio de Janeiro, Brasil.*
[*] *e-mail: wania@if.ufrj.br*
[c] *Chemistry Institute, Federal University of Rio de Janeiro, Rio de Janeiro, Brasil.*

Contents

S1 Data reduction principles

S1.1 Single ionization intensities

The single ionization intensities were extracted from a spectrum showing the first ions that reach the detector, while the double ionization intensities were extracted from a 2D-dimensional map that recorded the counts of the first and second ions in coincidence. The following convention is used for the single ionization: $N^{true}(Y^+)$ denotes the true number of events when the original ionized molecule dissociates into a neutral X and a Y^+ ion and $N^{mea}(Y^+)$ the number of measured events, and for the double ionization when an ion-ion pair X^+ and a Y^+ is created. The equations 1 to 3 below provide the true counts $N^{true}(Y^+)$ for the CFC and HCFC and reference gas (REF - Kr or Xe) ion species from the measured ones, $N^m(Y^+)$ and $N^m(X^+, Y^+)$, where Y stands for REF and ionic fragments of CFCs and X for H and $C\ F$ and Cl and, ε is the efficiency of the detection system for each ionic species. For single ionized CFCs, only the correction for detection efficiency applies:

$$N^{true}(CFC^+, REF^+) = \frac{N^{mea}(CFC^+, REF^+)}{\varepsilon_Y} \tag{1}$$

For single dissociative ionization two terms are needed:

$$N^{true}(Y^+) = \frac{N^m(Y^+)}{\varepsilon_Y} - \frac{(1-\varepsilon_X)}{\varepsilon_X \varepsilon_Y} \times N^{mea}(X^+, Y^+) \tag{2}$$

The first term corrects the single ionization counts concerning the ion detection efficiency, while the second one takes into account false counts from double ionization. If only one ion of an ion pair is detected, this contributes as a false event to the singles spectrum. It will be measured as a single charge event that produces an artificial enhancement of the single ionization channels. Not only is it necessary to correct for detection efficiencies, but also to subtract false events [1? –3]. The next equation corrects for the double ionization events for the ion-ion pair detection efficiencies. The true counts are enhanced much more than the single ionization events due to double detection efficiencies factors.

$$N^{true}(X^+, Y^+) = \frac{1}{\varepsilon_X \varepsilon_Y} \times N^{mea}(X^+, Y^+) \tag{3}$$

S1.2 Relative flow technique

Krypton and xenon were chosen for their mass proximity to CFC and HCFC to ensure homogeneity in the gas mixing ratio during molecular flow and for similar detection efficiency[4,5]. The cross-sections are defined as follows:

$$\frac{N_{CFC}^{true}}{N_{REF}^{true}} = \frac{\sigma_{CFC}}{\sigma_{REF}} \frac{\beta_{CFC}}{\beta_{REF}} \sqrt{\frac{M_{CFC}}{M_{REF}}} \tag{4}$$

where σ refers to the ionization cross-section, β is related to the volume of interaction defined by the intersection between the molecular beam and the electron beam[6], and M is the molecular weight. The mass factor represents the ratio of flow rates of the gases through the needle.

The beam profile of the molecular beam depends on the mean free path. The driving pressure P_s behind the needle should be such that the mean free paths are equal according to their diameters of gas-kinetics. CFC and HCFC and reference gases have similar atomic weights and gas kinetics[4,7], resulting in similar mass flow rates. The beam profiles of the two gases can be closely considered the same.

$$\frac{\beta_{CFC}}{\beta_{REF}} = \frac{R_{CFC}}{R_{REF}} \tag{5}$$

The relative flow rate R is related to the outflow of gases P_s from the reservoir in steady-state condition. In the intermediate flow regime, R is given by

$$R = aP_s(1 + \alpha P_s) \tag{6}$$

where the first and second terms are the rates due to the free-molecular and binary-collision processes, respectively[?]. For the range of driving pressures P_s where inter-atomic-molecular collisions within the tube are negligible, the constant factor a is inversely dependent on $\sqrt{M}$, the number of molar masses. The product $a\alpha$ is proportional to $\delta^2/\sqrt{M}$, where δ is the kinetic molecular diameter[4,7,8]. Equation 5 implies that a ratio and a pressure-dependent expression $1 + \alpha\ P_s$ in the numerator and denominator would not greatly change the results due to a nonlinear relationship between flow rate and pressure. The working pressures and lengths of the tubes and needle determine that the measurements are operated mainly in free molecular flow. The true intensities of CFC(HCFC) ions $N^{true}{}_{CFC}(E_i, Y)$ are

converted into absolute ionization cross-sections at electron energies E_i of the ion species Y as defined in equation 2.

$$\sigma_{CFC}(E_i,Y) = \sigma_{REF}(E_i,REF^+)\frac{N^{true}_{CFC}(E_i,Y)}{N^{true}_{REF}(E_i,REF^+)} \quad (7)$$

where the single ionization electron impact cross-sections of REF - Kr and Xe - are taken from Rejoub et al. $\sigma_{REF}(E_i,REF^+)$ [9–11], and the present measured true intensity of the single ionized REF^+, ($N^{true}_{REF}(E_i,REF^+)$ events, with efficiency ε_{REF^+} were considered for normalization (see equation 1).

S1.3 Detector efficiency

For the analysis of the relative cross sections for different ions, it must be considered that ions with a high mass/charge ratio are detected with a lower efficiency than those with lower ones. In the literature, several procedures are described to determine the detection efficiencies of *MCPs* [5,12–19]. In the present work, the detector efficiency approach recommended by Krems *et al*. was followed [5]. They provide an analytic formula to express the efficiencies for ions that scale to a single curve as a function of the impact energy divided by the square root of the ion mass [5,12].

S1.4 Mass resolution

For RIMs configuration: the mass resolution Δ at the mass 84 of krypton to its neighbor isotopic mass 83 is estimated to be 0.9 Although the mass resolution for the inertial reference gasses is good (the isotopic components of xenon and krypton were well discriminated), a superposition of ionic peaks is clearly observed for the chlorofluorocarbon's cations with a small mass difference. In contrast to the thermal energy of the inert gases the kinetic energies of fragment ions can be quite high, forming wide time of flight peaks that sometimes encompass two ionic radicals. The measurement with a reflectron spectrometer with high mass resolution was chosen to discriminate the contribution of these ionic species without the need of any the deconvolution procedure.

S1.5 Cross sections: present and literature data

A series of experimental works from different groups of chlorofluorocarbons have undergone successive re-measurements and reanalysis, as pointed out in the articles by Christophorou et al [20,21]. due to efficiency issues dealing with ion transmission, electron multiplier mass dependence, and pulse processing. All the issues that justify the present deviations

were discussed in the publication Absolute electron impact ionization cross-sections for CF4: Three-dimensional recoil-ion imaging combined with the relative flow technique[22]

Some points that are the most relevant concerning this issue are the following.

(i) In the case of ion-ion pair production, if one of the ions is not collected, it introduces double-ionization events into the single ionization. The detection of only one ion of an ion pair contributes as a "false" event to the single spectrum. The evaluation of single and double coincident ionization events allows the determination of the "false" events and the proper subtraction of their contribution (see the equation in S1.1). The correction values are given as percent for each ionic species in tables 2 and 4 of the main text for $CClF_3$ and $CHClF_2$ respectively. Therefore, without data reduction, the cross sections are overestimated.

(ii) Several groups apply corrections factors to account for reduced collection. Only experimental knowledge of the momentum/energy of each ejected ion can properly correct the loss of detection. Simulations to obtain correction factors without that information can overestimate the "true" ion counting rate of species ejected with different momentum/energy .

The spectra generated by the RIMS technique allow one to determine whether the conditions were set appropriate for the transmission/collection of all or mostly all ions irrespective of their momentum. The large MCPs of 80mm in diameter in chevron configuration assured a full 4π ion collection displayed in figure 2 of the main text[23,24].

(iii) Some works apply the RTF method to obtain the absolute cross sections[6,23,25–27] as in the present work. It is essential to select a reference molecule with similar mass. By choosing an inert gas with similar mass of $CClF_3$ and $CHClF_2$, xenon and krypton, respectively, allowed the consideration of thermodynamic arguments[7] and parameters for the consistent application of the RFT method[4,25]. The details of the technique are presented in detail in[22]and used in previous work on fluorocarbons[23].

S1.6 Uncertainties

The experimental uncertainties can relate to three procedures that yield in total 10-15%. 1. Data analysis: statistical and contribution of single and double events. 2. Relative flow technique (RFT), mainly Injection mixture pressure. 3. Recoil Ion Momentum spectroscopy technique (RIMS), collection efficiency, and detection efficiency

1) The accuracy limit of extracting ion intensities is estimated to be 5-7% as all ions were distinguished from each other by their time of flight (RIMSs and (TOF-Ref) and full momentum. In the case of hydrogenated ions, the

discrimination was performed with the help of the reflectron spectrometer, which avoided the deconvolution procedure to distinguish and extract the individual contribution of the ions intensities.

Finally, the determination of the intensities of the ions in single ionization events was corrected for false events coming from double ionization events (see discussion in SI)[1,3,22]. Without applying this correction in the single ion intensities, the major deviations will be present in the cross-section evaluation. The grid efficiency was already previously tested and is well known.

2) Conversion of the relative cross sections into absolute ones by RFT implies uncertainties in the density proportion of the gas mixture, which was well fixed by selecting a total gas pressure of 100 ml in the small container (3%) and subsequent transmission to the large container to reach thermodynamic equilibrium before injection. The mixed gaseous samples are homogeneously distributed and the flow rates are according to the mixing ratio tests[4]. The other sample parameters in the RFT equation were well established (see in detail the equation in SI). The larger uncertainty in the conversion can arise from the reference gas measurement and literature cross sections. The values of krypton and xenon in the literature are well accepted, and the experimental single- and multiple cross section ratios are verified against the ones of the literature (3%).

3) The transmission efficiency is very high due to the full 4 pi collection by the delay line detector of 80mm diameter. Only the atomic ions were mostly fully detected, but their cross sections were small. As is known, the MCPs efficiency depends on the ion mass (ion masses with high mass/charge ratio are usually detected with less efficiency compared to those with lower ones). Several procedures are listed in the literature, and we opt to adopt the approach recommended by Krems[5]. An analytical formula expresses the efficiencies of ions . Total uncertainty 5% .

S2 TOF-spectra

S2.1 TOF spectrum of $CClF_3$ and $CHClF_2$

In figure S1, the mass spectra of the molecules $CClF_3$ and $CHClF_2$ are shown for comparison. Both spectra were normalized at the Cl^+ ion peak.

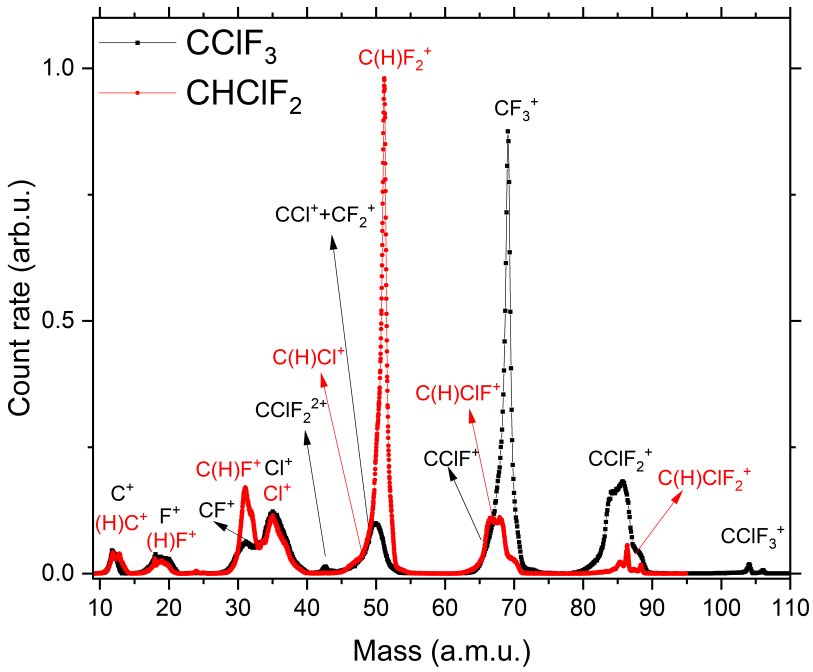

Figure S1 TOF spectrum for $CClF_3$ (black) and $CHClF_2$ (red) molecules at 200 eV for comparison. Both spectra normalized by the Cl^+ ion peak.

S2.2 Spectrum of $CHClF_2$

In figure S2, the mass spectra of the $CHClF_2$ molecule are divided into regions showing the relative intensities of the mass species with hydrogen preferentially attached to the radical species or without the hydrogen atom.

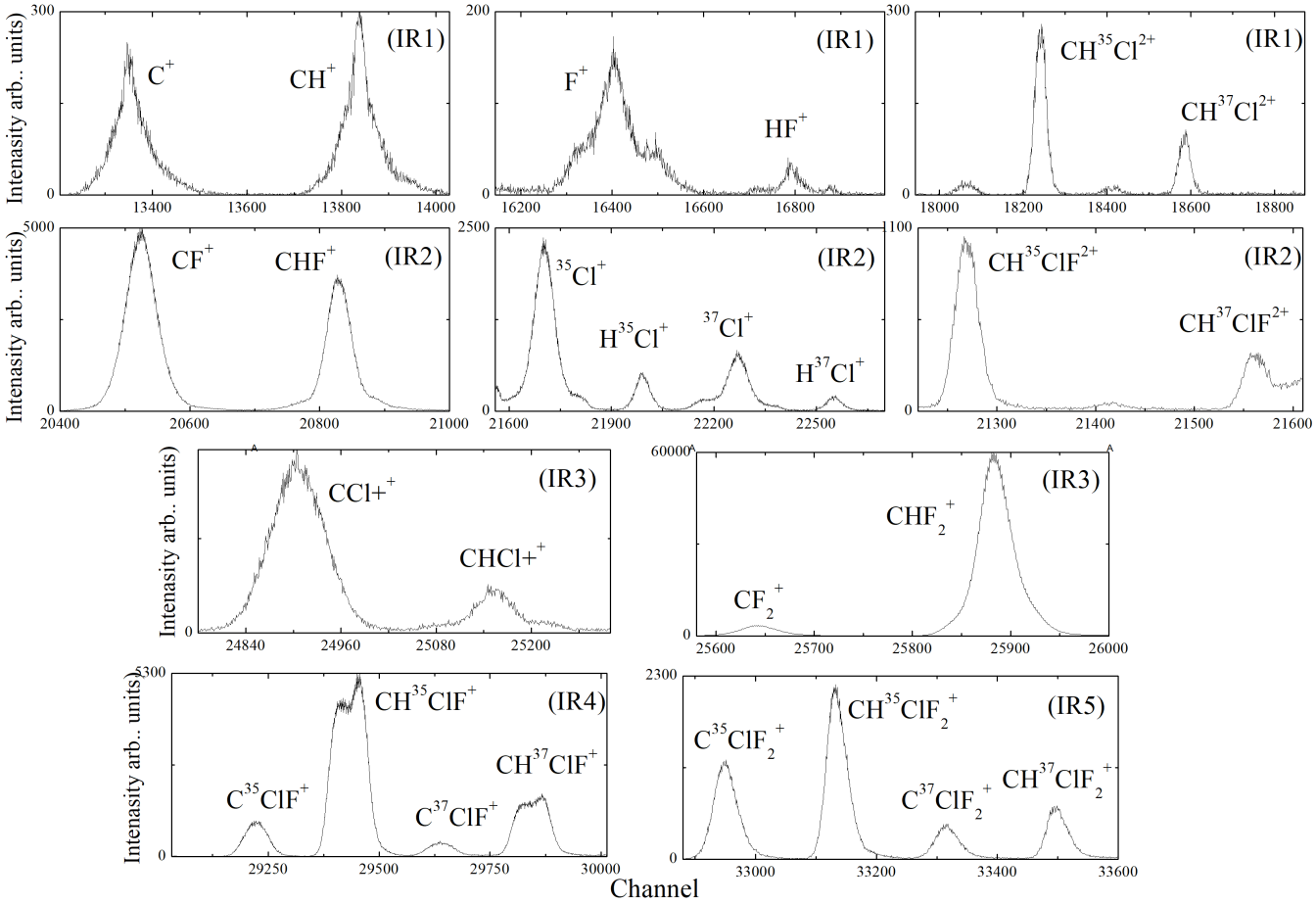

Figure S2 TOF spectrum for $CHClF_2$ at 200 eV.

S2.3 2D map of Y-position on the detector and time-of-flight (TOF) spectrum

The background was weak and well below of the line intensities. It can be clearly observed in the 2-dimensional spectra (a) with the Y-projection (b) shown in figures **??**for for 200 eV electron impact on CClF3 and CHClF2, respectively.

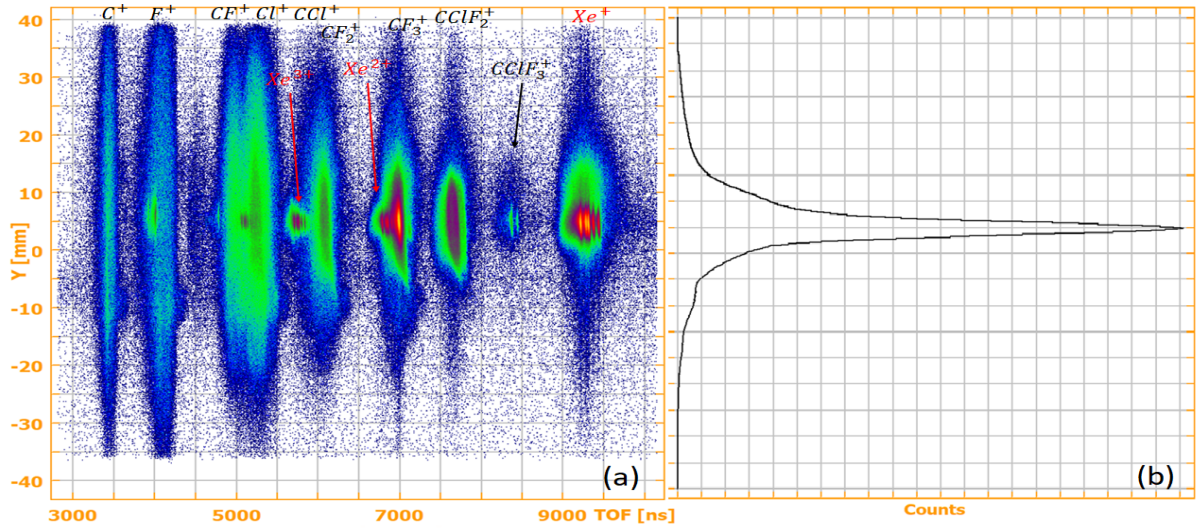

Figure S3 (left) 2D map of Y-position on the detector and time-of-flight (TOF) spectrum for $CClF_3$ at 200 eV. (right) Projection onto the Y-axis of the 2D spectrum.

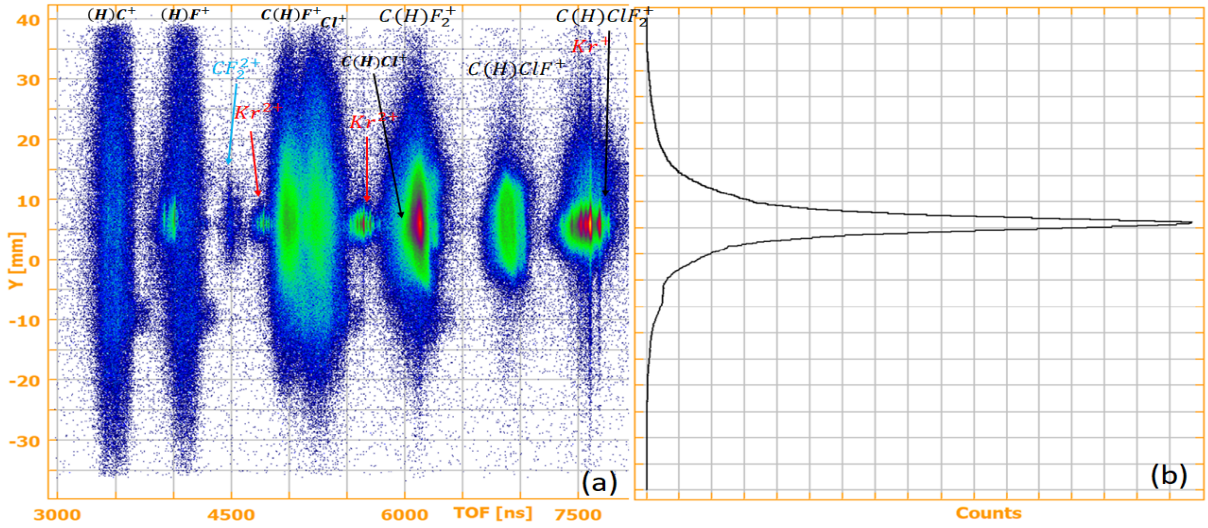

Figure S4 (left) 2D map of Y-position on the detector and time-of-flight (TOF) spectrum for $CHClF_2$ at 200 eV. (right) Projection onto the Y-axis of the 2D spectrum.

S3 Theoretical insights - Scan and NEB methods

The search for the Minimum Energy Path (MEP) between the initial structure (compound IS) and the final structure (compound FS) implies seeking for a mechanistic route from the IS to the FS. Both Scan and NEB (Nudged Elastic Band) methods were employed to identify the MEPs for the reactions investigated[28]. Both were calculated at the DFT level (PBE0/def2-TZVP).

1) In the case of dissociation, such as reaction R1 in Figure 15 in the main text, an atom is ejected from the molecule. The mechanistic route consists of breaking a bond, which is essentially what a Scan performs. The software is instructed to move two atoms apart by specifying the initial distance, the final distance, and the number of steps to be taken between these points. At each step, the remaining structure is optimized.
Since we are dealing with dissociation, the mechanistic route that minimizes the Potential Energy Surface (PES) between the compound IS and the compound FS is the separation of the two structures. However, after ejection, the molecular structure may undergo rearrangements; therefore, optimizations during this bond-breaking process are fundamental to describe the dissociation process. This is why the method is called a Potential Energy Relaxed Scan. Consequently, the bond distance in these scans reflects the initial and final distances between the previously bonded atoms (ions) and the intermediate points requested.

2) The case described in panel R2 in Figure 15 (main text) involves steps with processes distinct from simple dissociation, such as the formation of new bonds and the breaking of others. The Scan method works as an auxiliary tool to find reaction intermediates that assist in identifying the path minimizing the energy from compound IS to FS. However, the Scan method alone may not be ideal for describing the mechanism. In these cases, the NEB method (Nudged Elastic Band) is more appropriate to optimize the pathway between reactants IS and products FS. An initial path is generated, followed by a sequence of intermediate structures, referred to as images or reaction coordinates, that describe the reaction pathway. To determine the minimum energy path, an interaction is introduced between neighboring images linked by springs, forming an elastic band. A pre-selected number of steps were executed to transition from the reactant IS to the product FS iteratively adjusting the image positions along the band (along the reaction path) minimizing energy until a minimum energy pathway (MEP) was achieved.

Unlike the Scan method, where the reaction coordinate is limited to the distance between two structures, the NEB scans all coordinates and degrees of freedom. Each NEB optimization cycle involves the evaluation of the energy and gradient of images with geometries that describe the path connecting Is to FS. Since the NEB method does not operate along fixed points (like a distance between compound IS and FS) but explores all degrees of freedom, it is expressed in terms of Images—the points on the band connecting IS to FS along the minimum energy path.

S4 Environmental impact of $CClF_3$ and $CHClF_2$

$CClF_3$ has an Ozone Depletion Potential (ODP) of 0.82 and a Global Warming Potential (GWP) of 14,400 over a 100-year period. Furthermore, its long atmospheric lifetime and high GWP make it a potent greenhouse gas, far exceeding the impact of CO_2 considering equal concentrations. Although $CHClF_2$ has a lower ODP of 0.055, it still poses environmental concerns. Its GWP is 1,810 over a 100-year period, indicating its contribution to global warming despite being a temporary replacement for more harmful CFCs[29,30].

References

[1] M. Simon, T. LeBrun, P. Morin, M. Lavollée and J. Maréchal, *Nuclear Instruments and Methods in Physics Research Section B: Beam Interactions with Materials and Atoms*, 1991, **62**, 167–174.

[2] H. Luna, W. Wolff, E. C. Montenegro and L. Sigaud, *Phys. Rev. A*, 2019, **99**, 012709.

[3] W. Wolff, H. Luna, E. C. Montenegro and L. C. Rodrigues Junior, *Phys. Rev. A*, 2020, **102**, 052821.

[4] M. G. P. Homem, I. Iga, R. T. Sugohara, I. P. Sanches and M. T. Lee, *Review of Scientific Instruments*, 2011, **82**, 013109.

[5] M. Krems, J. Zirbel, M. Thomason and R. D. DuBois, *Review of Scientific Instruments*, 2005, **76**, 093305.

[6] M. J. Brunger and S. J. Buckman, *Physics Reports*, 2002, **357**, 215–458.

[7] F. E. Daneş, S. Daneş, V. Petrescu and E.-M. Ungureanu, in *Distribution of Molecular Properties in Gases*, Springer International Publishing, Cham, 2021, pp. 87–131.

[8] S. Kunze, R. Groll, B. Besser and J. Thöming, *Scientific Reports*, 2022, **12**, 2057.

[9] R. Rejoub, B. G. Lindsay and R. F. Stebbings, *Phys. Rev. A*, 2002, **65**, 042713.

[10] P. Nagy, A. Skutlartz and V. Schmidt, *Journal of Physics B: Atomic and Molecular Physics*, 1980, **13**, 1249.

[11] E. Krishnakumar and S. K. Srivastava, *Journal of Physics B: Atomic, Molecular and Optical Physics*, 1988, **21**, 1055.

[12] C. N. Burrous, A. J. Lieber and V. T. Zaviantseff, *Review of Scientific Instruments*, 1967, **38**, 1477–1481.

[13] K. Fehre, D. Trojanowskaja, J. Gatzke, M. Kunitski, F. Trinter, S. Zeller, L. P. H. Schmidt, J. Stohner, R. Berger, A. Czasch, O. Jagutzki, T. Jahnke, R. Dörner and M. S. Schöffler, *Review of Scientific Instruments*, 2018, **89**, 045112.

[14] B. Gaire, A. M. Sayler, P. Q. Wang, N. G. Johnson, M. Leonard, E. Parke, K. D. Carnes and I. Ben-Itzhak, *Review of Scientific Instruments*, 2007, **78**, 024503.

[15] S. Hosokawa, N. Takahashi, M. Saito and Y. Haruyama, *Review of Scientific Instruments*, 2010, **81**, 063301.

[16] N. Takahashi, Y. Adachi, M. Saito and Y. Haruyama, *Nuclear Instruments and Methods in Physics Research Section B: Beam Interactions with Materials and Atoms*, 2013, **315**, 51–54.

[17] J. Oberheide, P. Wilhelms and M. Zimmer, *Measurement Science and Technology*, 1997, **8**, 351.

[18] H. C. Straub, M. A. Mangan, B. G. Lindsay, K. A. Smith and R. F. Stebbings, *Review of Scientific Instruments*, 1999, **70**, 4238–4240.

[19] B. Brehm, J. Grosser, T. Ruscheinski and M. Zimmer, *Measurement Science and Technology*, 1995, **6**, 953.

[20] L. G. Christophorou and J. K. Olthoff, in *Assessed Total and Partial Ionization Cross Sections for CF4, C2F6, C3F8, CHF3, CF3I, c-C4F8, Cl2, CCl2F2, BCl3, SF6, and Fragments of CF4 and SF6*, ed. L. G. Christophorou, J. K. Olthoff and P. Vassiliou, Springer US, Boston, MA, 2004, pp. 173–180.

[21] L. G. Christophorou and J. K. Olthoff, *Journal of Physical and Chemical Reference Data*, 1999, **28**, 967–982.

[22] W. Wolff, M. Dogan, H. Luna, L. H. Coutinho, D. Mootheril, W. Baek, T. Pfeifer and A. Dorn, *Review of Scientific Instruments*, 2024, **95**, 095103.

[23] M. Dogan, W. Wolff, D. M. Mootheril, T. Pfeifer and A. Dorn, *Phys. Chem. Chem. Phys.*, 2025, **27**, 10057–10072.

[24] O. Jagutzki, V. Mergel, K. Ullmann-Pfleger, L. Spielberger, U. Spillmann, R. Dörner and H. Schmidt-Böcking, *Nuclear Instruments and Methods in Physics Research Section A: Accelerators, Spectrometers, Detectors and Associated Equipment*, 2002, **477**, 244–249.

[25] M. G. P. Homem, R. T. Sugohara, I. P. Sanches, M. T. Lee and I. Iga, *Phys. Rev. A*, 2009, **80**, 032705.

[26] M. A. Khakoo, K. Keane, C. Campbell, N. Guzman and K. Hazlett, *Journal of Physics B: Atomic, Molecular and Optical Physics*, 2007, **40**, 3601.

[27] J. C. Nickel, P. W. Zetner, G. Shen and S. Trajmar, *Journal of Physics E: Scientific Instruments*, 1989, **22**, 730.

[28] F. Neese, *Wiley Interdiscip. Rev. Comput. Mol. Sci.*, 2012, **2**, 73–78.

[29] M. Prignon, S. Chabrillat, D. Minganti, S. O'Doherty, C. Servais, G. Stiller, G. C. Toon, M. K. Vollmer and E. Mahieu, *Atmospheric Chemistry and Physics*, 2019, **19**, 12309–12324.

[30] M. Chirkov, G. P. Stiller, A. Laeng, S. Kellmann, T. von Clarmann, C. D. Boone, J. W. Elkins, A. Engel, N. Glatthor, U. Grabowski, C. M. Harth, M. Kiefer, F. Kolonjari, P. B. Krummel, A. Linden, C. R. Lunder, B. R. Miller, S. A. Montzka, J. Mühle, S. O'Doherty, J. Orphal, R. G. Prinn, G. Toon, M. K. Vollmer, K. A. Walker, R. F. Weiss, A. Wiegele and D. Young, *Atmospheric Chemistry and Physics*, 2016, **16**, 3345–3368.